

Contents lists available at ScienceDirect

### Water Research

journal homepage: www.elsevier.com/locate/watres





## Aggregation kinetics and stability of biodegradable nanoplastics in aquatic environments: Effects of UV-weathering and proteins

Yingxue Yu<sup>a</sup>, Anton F. Astner<sup>b</sup>, Tahsin Md. Zahid<sup>c</sup>, Indranil Chowdhury<sup>c</sup>, Douglas G. Hayes<sup>b</sup>, Markus Flury<sup>a,\*</sup>

- <sup>a</sup> Department of Crop & Soil Sciences, Washington State University, Puyallup and Pullman, WA, USA
- b Department of Biosystems Engineering and Soil Science, The University of Tennessee, Knoxville, TN, USA
- <sup>c</sup> Department of Civil and Environmental Engineering, Washington State University, Pullman, WA, USA

### ARTICLE INFO

# Keywords: Biodegradable nanoplastics Polybutylene adipate co-terephthalate (PBAT) Aggregation Protein Weathering Natural water

### ABSTRACT

Plastic pollution caused by conventional plastics has promoted the development and use of biodegradable plastics. However, biodegradable plastics do not degrade readily in water; instead, they can generate microand nanoplastics. Compared to microplastics, nanoplastics are more likely to cause negative impacts to the aquatic environment due to their smaller size. The impacts of biodegradable nanoplastics highly depend on their aggregation behavior and colloidal stability, which still remain unknown. Here, we studied the aggregation kinetics of biodegradable nanoplastics made of polybutylene adipate co-terephthalate (PBAT) in NaCl and CaCl<sub>2</sub> solutions as well as in natural waters before and after weathering. We further studied the effect of proteins on aggregation kinetics with both negative-charged bovine serum albumin (BSA) and positivecharged lysozyme (LSZ). For pristine PBAT nanoplastics (before weathering), Ca<sup>2+</sup> destabilized nanoplastic suspensions more aggressively than Na+, with the critical coagulation concentration being 20 mM in CaCl2 vs 325 mM in NaCl. Both BSA and LSZ promoted the aggregation of pristine PBAT nanoplastics, and LSZ showed a more pronounced effect. However, no aggregation was observed for weathered PBAT nanoplastics under most experimental conditions. Further stability tests demonstrated that pristine PBAT nanoplastics aggregated substantially in seawater, but not in freshwater, and only slightly in soil pore water; while weathered PBAT nanoplastics remained stable in all natural waters. These results suggest that biodegradable nanoplastics, especially weathered biodegradable nanoplastics, are highly stable in the aquatic environment, even in the marine environment.

### 1. Introduction

Plastic has become a serious pollutant in the environment. It was reported that approximately 8300 million metric tons of plastics were produced by 2017, and 4900 million metric tons were discarded in landfills or the natural environment (Geyer et al., 2017). These discarded plastics threaten ecosystems, not only by themselves but also by the generated micro- and nanoplastics during breakdown. Large plastic pieces can entangle animals in land and in water, leading to reduced mobility and starvation (Law, 2017; Ryan, 2018), while micro- and nanoplastics can be ingested and inhaled by animals, causing decreased food uptake, impeded growth, and inflammation (Cole and Galloway, 2015; Espinosa et al., 2018; Prata, 2018). To alleviate these problems, biodegradable plastics have been proposed to replace conventional plastics, particularly for single-use plastics. Unlike conventional plastics, which are persistent and can reside in the environment for decades

or even centuries (Nithin and Goel, 2017), biodegradable plastics can degrade completely in months or years when disposed of in appropriate environments (Narancic et al., 2018; Tosin et al., 2019; Sintim et al., 2020).

Although biodegradable plastics can be metabolized by microorganisms and be converted into  $\mathrm{CO}_2$ ,  $\mathrm{CH}_4$ , and biomass (Haider et al., 2019; Flury and Narayan, 2021), they inevitably generate micro- and nanoplastics during degradation (González-Pleiter et al., 2019; Sintim et al., 2019). The generated micro- and nanoplastics will unlikely pose an environmental threat, if biodegradable plastic waste is appropriately managed and disposed of in industrial composting or anaerobic digestion facilities, where full degradation of the plastics can be reached before the generated micro- and nanoplastics are released to the environment (Kubowicz and Booth, 2017; Yu et al., 2021). However,

<sup>\*</sup> Corresponding author.

E-mail address: flury@wsu.edu (M. Flury).

mismanagement or off-site transport can happen, leading to exposure of biodegradable plastics and thus to the release of micro- and nanoplastics to the environment.

Exposure of biodegradable plastics to the aquatic environment can be especially concerning. As shown in previous studies, biodegradable plastics made of polybutylene adipate co-terephthalate (PBAT) did not readily degrade in water (Wang et al., 2019), instead, they generated more microplastics than low-density polyethylene plastics (Wei et al., 2021). These generated biodegradable microplastics may persist and accumulate in the aquatic environment and further fragment into secondary nanoplastics. Secondary nanoplastics were indeed found to be released from biodegradable microplastics made of polyhydroxy-butyrate when the microplastics were immersed in water, and these nanoplastics further induced decrease in cellular growth and altered physiological parameters of freshwater cyanobacterium, alga, and crustacean (González-Pleiter et al., 2019). This raises concerns about the impacts of secondary biodegradable nanoplastics in the aquatic environment.

The impacts of secondary nanoplastics on aquatic ecosystems depend on the nanoplastics' aggregation behavior and colloidal stability. Aggregation and stability of nanoplastics have been intensively studied with model polystyrene nanoplastics (Liu et al., 2019; Wang et al., 2020; Li et al., 2021b), but only a few studies with other types of polymers exist (Shams et al., 2020). These studies show that particle–particle interactions are controlled by surface properties and solution chemistry. Surface properties of nanoplastics can be modified by weathering, which increases the negative charge of nanoplastics and inhibits aggregation (Liu et al., 2019; Wang et al., 2020). Besides, extracellular polymeric substances, such as proteins can cover nanoplastics with a corona, which can either hinder aggregation through imposing steric repulsion or promote aggregation through decreasing electrostatic interaction (Li et al., 2021b).

However, to the best of our knowledge, no information is currently available about the effects of weathering and proteins on aggregation of biodegradable nanoplastics. To fill this knowledge gap, we studied the aggregation behavior of biodegradable nanoplastics generated from a PBAT mulch film. The PBAT mulch film was chosen because PBAT is the most commonly used polymer in biodegradable plastic mulch films, which are intentionally introduced into the environment through soilincorporation. The aggregation of PBAT nanoplastics before and after weathering was examined in both NaCl and CaCl<sub>2</sub> solutions (Na<sup>+</sup>, Ca<sup>2+</sup>, and Cl<sup>-</sup> represent common ions in natural water). The effect of proteins was studied with negative-charged bovine serum albumin (BSA) and positive-charged lysozyme (LSZ). Both BSA and LSZ are abundant in natural waters and have been commonly used as model proteins to study the interaction between nanoplastics and proteins (Dong et al., 2020; Li et al., 2021a,b). Further, we determined the stability of PBAT nanoplastics in soil pore water, freshwater, and seawater, to estimate the potential of biodegradable nanoplastics to migrate from land to oceans. We hypothesized that (1) weathering stabilizes PBAT nanoplastics, (2) proteins promote the aggregation of PBAT nanoplastics, and (3) PBAT nanoplastics are highly stable in natural waters.

### 2. Materials and methods

### 2.1. Pristine and weathered PBAT nanoplastics

A biodegradable plastic mulch film made of polybutylene adipate co-terephthalate (PBAT, BioAgri, BioBag Americas, Dunedin, FL) was used to generate PBAT nanoplastics. The PBAT mulch film was black with a thickness of 29  $\pm$  1.2  $\mu m$  and a density of 22.8  $\pm$  0.4 g m $^{-2}$  (further properties of the film are given in Hayes et al. (2017)). Briefly, film pieces (12 cm  $\times$  2 cm) were cut off from a new roll of mulch film, sequentially soaked in deionized water and liquid nitrogen, and then blended, milled, sieved, wet ground, and air-dried (Astner et al.,

2019). The resulting mulch powder (7 g) was suspended in deionized water, filtered through a 0.45  $\mu m$  membrane filter (HAWP04700, MF-Millipore, MilliporeSigma, Burlington, MA), and then through a 0.22  $\mu m$  syringe filter (SLGP033RB, Millex-GP, Merck Millipore Ltd., Ireland). The filtrate was collected as the stock suspension of pristine PBAT nanoplastics. The stock suspension had a concentration of about 470 mg/L (based on gravimetric analysis).

The stock suspension of weathered PBAT nanoplastics was prepared from UV-weathered ground mulch powder. An aliquot (7 g) of the ground mulch powder was irradiated with a 1 kW xenon arc lamp (wavelength: 300-800 nm, 650 W/m²) in an Atlas SunTest CPS+ solar simulator (Atlas Material Testing Technology LLC, Mount Prospect, IL) for 336 h. The 336-h exposure is equivalent to 66 days of European mean solar irradiance (Gewert et al., 2018), which represents the sunlight exposure of biodegradable plastic mulch films during growing seasons. The sample was placed into a Pyrex glass beaker (200 mL) and manually mixed every 24 h to ensure uniform weathering. Then, the sample was suspended in deionized water and filtered sequentially through 0.45  $\mu$ m membrane filters and 0.22  $\mu$ m syringe filters to collect filtrate containing weathered PBAT nanoplastics, and the filtrate had a concentration of about 380 mg/L (gravimetrically determined).

#### 2.2. Characterization of pristine and weathered PBAT nanoplastics

The morphology and size of pristine and weathered PBAT nanoplastics were visualized with scanning electron microscopy (SEM, FEI Apreo VolumeScope SEM, FEI Company, Hillsboro, OR). Briefly, a suspension (150 mg/L) of either pristine or weathered PBAT nanoplastics was sonicated for 10 min (Branson Ultrasonicator B-52, 50/60 Hz, 440 Watts) to break up any aggregates and disperse nanoplastics, and a drop (5  $\mu$ L) was deposited onto a SEM stub, air-dried in vacuum for 20 min, gold-coated, and imaged with SEM. The hydrodynamic diameters of pristine and weathered PBAT nanoplastics in deionized water (to obtain the intrinsic size) were measured with a Zetasizer Nano ZS (Malvern Instruments Ltd., Malvern, UK). To study the effect of pH, the  $\zeta$ potentials were measured in 10 mM NaCl with the Zetasizer over a wide range of pH (3 to 11, pH adjusted with 10 mM HCl or 10 mM NaOH). The effect of weathering was characterized with Raman spectroscopy (LabRAM, Horiba, Kyoto, Japan). The Raman spectra of both pristine and weathered PBAT mulch powder were collected using a 633 nm He-Ne laser with a  $50 \times$  objective (numerical aperture = 0.75).

### 2.3. Determination of aggregation kinetics

The aggregation kinetics of pristine and weathered PBAT nanoplastics were measured with the Zetasizer using the time-resolved dynamic light scattering in NaCl (10 mM to 1000 mM) and CaCl2 (2 mM to 50 mM) solutions (detailed experimental conditions are given in Table S1). Prior to the measurement, the stock suspensions of PBAT nanoplastics and the electrolyte solutions were adjusted to the same pH using 10 mM HCl or NaOH. For each measurement, the stock suspension of PBAT nanoplastics was sonicated for 10 min, and then aliquots of the stock suspension, deionized water, and electrolyte solution were pipetted into a disposable plastic cuvette to achieve desired nanoplastic and electrolyte concentrations (150 mg/L for both pristine and weathered PBAT nanoplastics, the concentration was chosen to ensure a good signal from the dynamic light scattering measurement). The cuvette was briefly vortexed for 3 s and placed into the Zetasizer, and dynamic light scattering measurement in terms of hydrodynamic diameter (Dh) was immediately carried out at 25 °C with the autocorrelation function accumulated for 2 min and continued for 50 min to obtain aggregation profiles. Each measurement was conducted in

The initial aggregation rate constant (k) of PBAT nanoplastics was determined as the slope of the linear least squares regression of the aggregation profiles up to the point where  $D_h(t)$  increased to

1.5  $D_h(t = 0)$ , because k is proportional to the initial rate of increase in  $D_h$  with time (Holthoff et al., 1996; Chen et al., 2006; Berg, 2010):

$$k \propto \frac{1}{N_0} \left( \frac{\mathrm{dD_h}(t)}{\mathrm{d}t} \right)_{t \to 0}$$
 (1)

where  $N_0$  is the initial nanoplastic concentration. To quantify the aggregation kinetics, the attachment efficiency ( $\alpha$ ) was calculated by normalizing the initial aggregation rate constant (k) by the initial aggregation rate constant under diffusion-limited (fast) aggregation condition ( $k_{\rm fast}$ ) (Chen et al., 2006; Berg, 2010):

$$\alpha = \frac{k}{k_{\text{fast}}} = \frac{\frac{1}{N_0} \left(\frac{\text{dD}_{\text{h}}(t)}{\text{d}t}\right)_{t \to 0}}{\frac{1}{N_{0, \text{fast}}} \left(\frac{\text{dD}_{\text{h}}(t)}{\text{d}t}\right)_{t \to 0, \text{fast}}}$$
(2)

where  $N_{0, \text{ fast}}$  was equal to  $N_0$  in the aggregation experiments. The critical coagulation concentration (CCC) was then determined as the electrolyte concentration where the extrapolated linear regression line of  $\alpha$  values in reaction-limited regimes intersects with  $\alpha=1$  in diffusion-limited regimes in logarithmic coordinates (Berg, 2010; Yang et al., 2019).

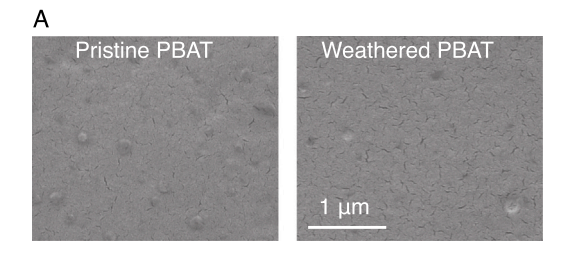
To study the effect of proteins, suspensions of negative-charged bovine serum albumin (BSA, molecular weight = 66.5 kDa, isoelectric point is pH 4.7, A8806, MilliporeSigma, Burlington, MA) and positive-charged lysozyme (LSZ, molecular weight = 14.3 kDa, isoelectric point is pH 11, L6876, MilliporeSigma, Burlington, MA) were prepared using deionized water with pH adjusted to the same value as the PBAT nanoplastic suspensions and the electrolyte solutions. After sonicating suspensions of PBAT nanoplastics and proteins separately (10 min), aliquots of PBAT nanoplastics, proteins, and electrolyte were pipetted into a disposable plastic cuvette to achieve desired protein and electrolyte concentrations, and dynamic light scattering measurements were carried out immediately after vortexing. Aggregation profiles of pristine and weathered PBAT nanoplastics were obtained in the presence of a fixed concentration of proteins (BSA or LSZ, 10 mg/L) in NaCl and CaCl<sub>2</sub> solutions. In the presence of BSA, a monotonic increase in k was found as the electrolyte concentration increases, thus  $\alpha$  was calculated in the same way as in the absence of proteins, and CCC values with BSA were further determined; while in the presence of LSZ, k generally decreased as the electrolyte concentration increased, thus  $\alpha$  was calculated with  $k_{\rm fast}$  being the initial aggregation rate constant of PBAT nanoplastics at the lowest electrolyte concentration. Besides, we obtained aggregation profiles of pristine and weathered PBAT nanoplastics at electrolyte concentrations close to CCC (NaCl and CaCl<sub>2</sub>) with different concentrations of proteins (BSA or LSZ, 2, 5, 10, 20, and 50 mg/L).

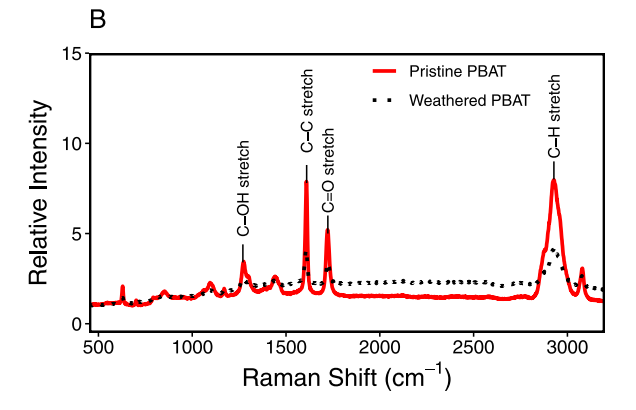
### 2.4. Derjaguin-Landau-Verwey-Overbeek (DLVO) interaction

The Derjaguin–Landau–Verwey–Overbeek (DLVO) theory was used to calculate the total interaction energy between PBAT nanoplastics. Both the classical DLVO theory and the extended DLVO theory including the Lewis acid–base interaction were used. Details are given in Section S1.

### 2.5. Stability of PBAT nanoplastics in different natural water

The stability of PBAT nanoplastics was studied by measuring hydrodynamic diameter of both pristine and weathered PBAT nanoplastics (150 mg/L) in different natural water samples. Three types of natural water samples were used: (1) soil pore water, (2) freshwater (Clark Creek, Puyallup, WA), and (3) seawater (Puget Sound, Tacoma, WA). The soil pore water was prepared by extracting soil water from saturated soil cores at 330 hPa with a ceramic pressure plate in a pressure chamber (Soil Moisture Equipment Corp., Santa Barbara, CA). The soil (silt loam) was collected from an agricultural field at the Washington State University (WSU) Puyallup Research and Extension





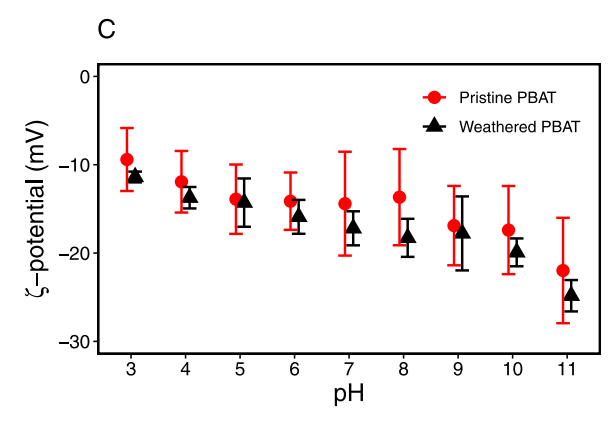


**Fig. 1.** Characteristics of pristine and weathered PBAT nanoplastics. (A) SEM images of pristine (left) and weathered (right) PBAT nanoplastics; (B) Raman spectra of pristine and weathered PBAT mulch powder; (C)  $\zeta$ -potentials of pristine and weathered PBAT nanoplastics in 10 mM NaCl solution at different pH (mean  $\pm$  standard deviation, n=6).

Center, and saturated overnight with rainfall water collected from the field (between March 15, 2022 to April 14, 2022). All water samples were filtered through 0.22  $\mu m$  membrane filters (GSWP04700, MF-Millipore, MilliporeSigma, Burlington, MA) after collection, and the chemical composition of these water samples is summarized in Table S2.

### 3. Results and discussion

### 3.1. Characterization of pristine and weathered PBAT nanoplastics

The SEM images show that both pristine and weathered PBAT nanoplastics were roughly spherical in shape, with sizes of  $128 \pm 4$  nm and  $142 \pm 8$  nm, respectively (mean  $\pm$  standard deviation, n=50, Fig. 1A). The sizes determined from SEM images matched the hydrodynamic diameters measured with the dynamic light scattering, which were  $140 \pm 7$  nm and  $152 \pm 39$  nm for pristine and weathered PBAT nanoplastics, respectively. The difference in size for the pristine and weathered PBAT nanoplastics can be attributed to the nanoplastic generation method, which could not produce identical particle sizes.

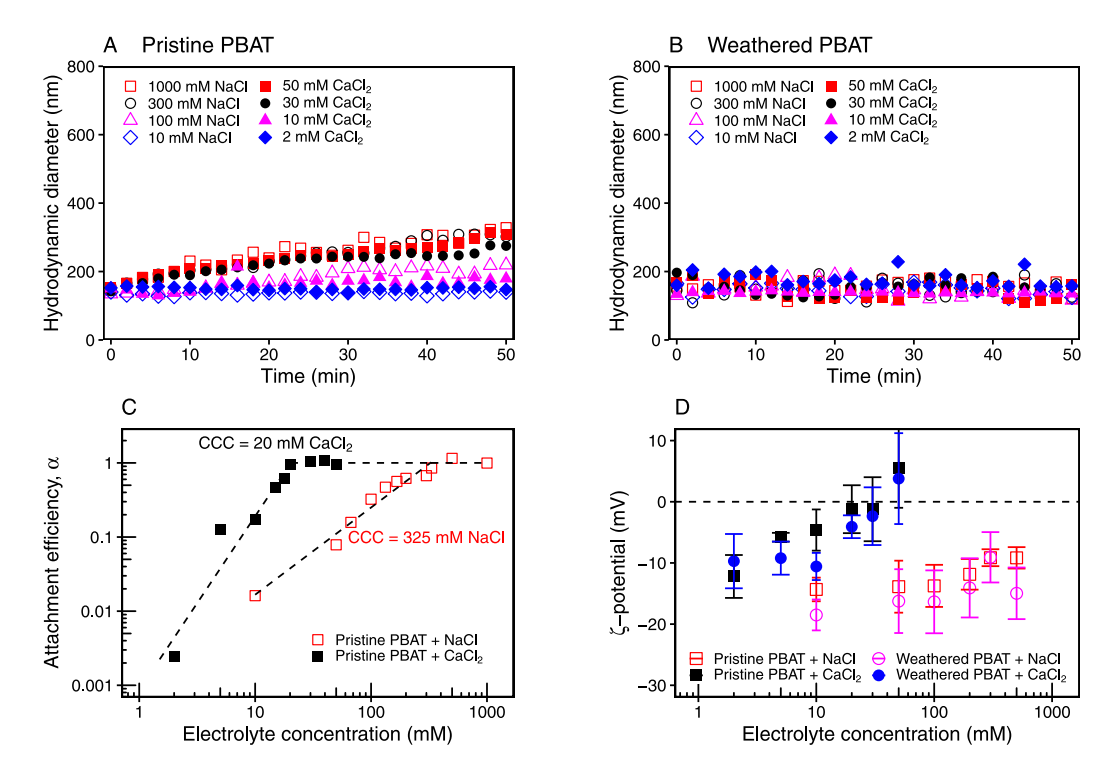


Fig. 2. Aggregation kinetics of pristine and weathered PBAT nanoplastics in NaCl and CaCl<sub>2</sub>. (A) Aggregation profiles of pristine PBAT nanoplastics; (B) aggregation profiles of weathered PBAT nanoplastics; (C) attachment efficiency (α) of pristine PBAT nanoplastics as a function of electrolyte concentrations; (D) ζ-potentials of pristine and weathered PBAT nanoplastics as a function of electrolyte concentrations. Aggregation profiles show the average of two replicates (only a subset of the aggregation profiles is given here for illustration purposes and the complete set is shown in Figure S1). ζ-potentials show mean  $\pm$  standard deviation of six measurements.

The Raman spectra revealed that the simulated solar exposure caused weathering of PBAT mulch powder, as the relative intensity of the characteristic peaks for the weathered PBAT mulch powder decreased at 1270 cm<sup>-1</sup> (C-OH stretch), 1610 cm<sup>-1</sup> (C-C stretch), 1723 cm<sup>-1</sup> (C=O stretch), 2928 cm<sup>-1</sup> (C-H stretch), compared to that for the pristine PBAT mulch powder (Fig. 1B). Both the pristine and the weathered PBAT nanoplastics were negatively charged at pH ranging from 3 to 11, while the weathered PBAT nanoplastics were slightly more negatively charged (Fig. 1C), which can be attributed to the relative abundance of C=O stretch in the weathered PBAT (Liu et al., 2019; Mistretta et al., 2019). As pH increases, both the pristine and the weathered PBAT nanoplastics became more negatively charged; but in the pH range of 5–8, typical for aquatic environments, their  $\zeta$ -potentials remained relatively constant, suggesting that the aggregation behavior of these nanoplastics is unlikely to be affected by pH in natural aquatic systems. Therefore, in this study, we carried out the aggregation kinetic experiments with a pH of  $6.0 \pm 0.3$ .

### 3.2. Aggregation kinetics of pristine and weathered PBAT nanoplastics in NaCl and $CaCl_2$

The aggregation profiles show that the aggregation of pristine PBAT nanoplastics was promoted by increasing concentration of electrolytes, while the aggregation of weathered PBAT nanoplastics was not affected (Fig. 2A,B). For the pristine PBAT nanoplastics, the hydrodynamic diameters remained unchanged at low concentrations of NaCl (<50 mM) and CaCl<sub>2</sub> (<10 mM); when the concentrations of NaCl and CaCl<sub>2</sub> exceeded 67 mM and 15 mM, respectively, the hydrodynamic diameters gradually increased over time (Figure S1A,B). The aggregation rate, as reflected by the attachment efficiency  $\alpha$ , increased with increasing electrolyte concentrations (Fig. 2C). As the concentrations of electrolyte further increased to the CCC, i.e., 325 mM NaCl and 20 mM CaCl<sub>2</sub>, the aggregation process changes from reaction-limited to diffusion-limited and  $\alpha$  became constant.

Such an aggregation behavior suggests that DLVO interactions controlled the aggregation of pristine PBAT nanoplastics. In the reaction-limited regime, i.e., electrolyte concentrations < CCC, the aggregation of particles is dominated by the repulsive electrical double layer forces. Indeed, under lower electrolyte concentrations, the  $\zeta$ -potentials of pristine PBAT nanoplastics were more negatively charged (Fig. 2D), and the classical DLVO calculation indicated the presence of an energy barrier, thus an overall repulsive interaction between PBAT nanoplastics (Figure S2A). While in the diffusion-limited regime, i.e., electrolyte concentrations > CCC, the energy barrier disappeared, and the interaction became attractive (Figure S2A).

However, the classical DLVO theory could not perfectly predict the aggregation of pristine PBAT nanoplastics. For instance, at 100 mM NaCl and 10 mM CaCl<sub>2</sub>, where the aggregation of pristine PBAT nanoplastics was reaction-limited, the total interaction energy was calculated to be attractive (Figure S2A). Such a discrepancy can be attributed to the assumption that particles are perfect spheres with the surface charge uniformly distributed in the DLVO theory. In addition, non-DLVO forces, such as hydrophobicity, could be accountable; however, the extended DLVO theory including the Lewis acid–base free energy predicted the interaction to be attractive under all electrolyte concentrations (Figure S2B), suggesting a negligible effect of surface hydrophobicity on the aggregation of pristine PBAT nanoplastics.

Compared to Na<sup>+</sup>, Ca<sup>2+</sup> was more effective to induce aggregation of pristine PBAT nanoplastics, which is expected due to the more effective charge neutralization and charge screening of Ca<sup>2+</sup> (Yang et al., 2019; Li et al., 2021b). Indeed, pristine PBAT nanoplastic were less negatively charged in CaCl<sub>2</sub> than in NaCl (Fig. 2D). The CCC ratio of Ca<sup>2+</sup>/Na<sup>+</sup> was 2<sup>-4</sup>, and agrees well with the Schulze–Hardy rule (i.e., 2<sup>-6</sup> to 2<sup>-2</sup>) (Elimelech et al., 1995), confirming that Ca<sup>2+</sup> is more effective to destabilize pristine PBAT nanoplastics. The more effective destabilization of Ca<sup>2+</sup> did not cause an obvious difference in the aggregate size, with the largest aggregate being 344 nm in NaCl and 312 nm in CaCl<sub>2</sub> at 50 min (Figure S1A,B).

Y. Yu et al. Water Research 239 (2023) 120018

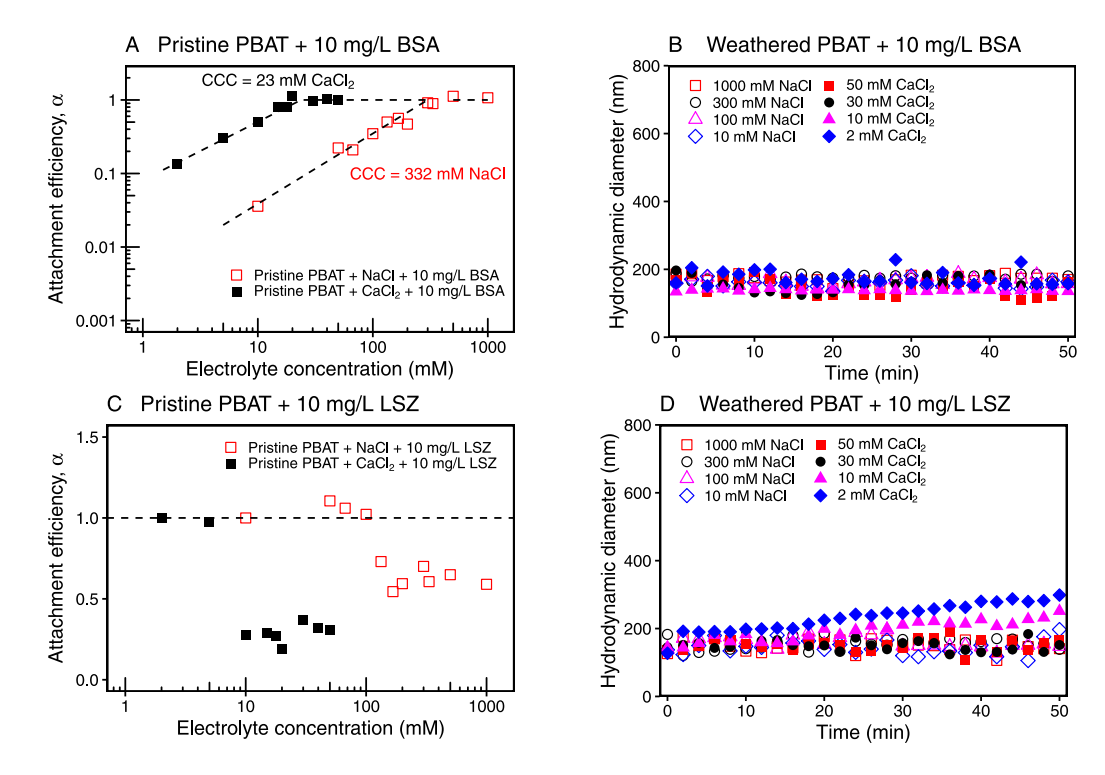


Fig. 3. Aggregation kinetics of pristine and weathered PBAT nanoplastics in the presence of 10 mg/L BSA or 10 mg/L LSZ as a function of NaCl and CaCl<sub>2</sub> concentration. (A) Attachment efficiency (a) of pristine PBAT nanoplastics in the presence of 10 mg/L BSA; (B) aggregation profiles of weathered PBAT nanoplastics in the presence of 10 mg/L BSA; (C) attachment efficiency (a) of pristine PBAT nanoplastics in the presence of 10 mg/L LSZ; (D) aggregation profiles of weathered PBAT nanoplastics in the presence of 10 mg/L LSZ. Aggregation profiles show the average of two replicates (only a subset of the aggregation profiles is given here for illustration purposes and the complete set is shown in Figure S3 and S6).

In contrast to the pristine PBAT nanoplastics, the hydrodynamic diameters of weathered PBAT nanoplastics remained unchanged over the whole range of electrolyte concentrations (Figure S1C,D), indicating that weathered PBAT nanoplastics were highly stable. Higher stability of particles is generally associated with more negative surface charges and thus stronger repulsive electrical double layer forces. Indeed, weathered PBAT nanoplastics were more negatively charged, as indicated by the  $\zeta$ -potentials (Fig. 2D), likely due to the abundance of oxygen-containing functional group (i.e., C=O). However, the negative charge of weathered PBAT nanoplastics alone could not explain their high stability, given that both the classical and extended DLVO calculations showed no obvious differences between pristine and weathered PBAT nanoplastics in terms of the total interaction energy (Figure S2). In addition to surface charge, surface roughness has been reported to contribute profoundly to colloid stability (Badaire et al., 2008; Lan et al., 2018). It is thus likely that the UV-weathering process induced roughening of PBAT nanoplastic surfaces, as was reported for other plastics (Qin et al., 2022).

### 3.3. Aggregation of pristine and weathered PBAT nanoplastics in the presence of bovine serum albumin (BSA)

Figure S3A,B shows the aggregation profiles of pristine PBAT nanoplastics in the presence of 10 mg/L BSA in NaCl and CaCl<sub>2</sub>. Compared to the absence of BSA, pristine PBAT nanoplastics became destabilized at lower electrolyte concentrations, i.e., 50 mM NaCl and 2 mM CaCl<sub>2</sub>, and grew into larger aggregate at higher electrolyte concentrations, i.e., 413 nm in NaCl and 452 nm in CaCl<sub>2</sub>. This indicates that the presence of 10 mg/L BSA promoted the aggregation of pristine PBAT nanoplastics at both low and high electrolyte concentrations. However, the presence of BSA barely changed the CCC in NaCl nor in CaCl<sub>2</sub>, which was 332 mM NaCl and 23 mM CaCl<sub>2</sub> (Fig. 3A).

The aggregation of pristine PBAT nanoplastics apparently followed a typical DLVO-type aggregation in the presence of BSA, suggesting the

dominant role of electrical double layer forces. Indeed, the  $\zeta$ -potentials of PBAT nanoplastics generally became less negative with increasing electrolyte concentrations (Figure S4A), leading to more attractive interactions between PBAT nanoplastics in the presence of BSA (Figure S4B). In addition, BSA can induce attractive patch-charge interaction and thus promote the aggregation of PBAT nanoplastics, as previously reported for hematite nanoparticles and polystyrene nanoplastics (Sheng et al., 2016; Li et al., 2021b).

Unlike our findings, previous studies have reported that BSA tends to stabilize single-walled carbon nanotubes, MnO2 colloids, and polystyrene nanoplastics through imposing steric repulsion (Saleh et al., 2010; Huangfu et al., 2013; Li et al., 2021a). However, steric repulsion can only become important when particles are fully and uniformly covered by BSA. Unfortunately, we could not quantify the absorbed amount of BSA on PBAT nanoplastics by centrifugation due to their small size and low density. But we found that the presence of BSA at low concentrations (< 10 mg/L) promoted the aggregation of pristine PBAT nanoplastics, while further increase in BSA concentrations showed a less promoting effect (Figure S5A,B). This is likely due to the attractive patch-charge interactions caused by the uneven and incomplete coverage of PBAT nanoplastics by BSA, resulting in BSA-rich areas of PBAT nanoplastics encounter BSA-poor areas of other PBAT nanoplastics (Li et al., 2021b). Further, the attractive patch-charge interactions become less pronounced with increasing BSA concentrations, as more surface area of PBAT nanoplastics became covered by BSA. BSA can also induce the aggregation of PBAT nanoplastics through bridging flocculation, where a polymer chain of BSA interacts with more than one nanoplastics and therefore leads to the formation of aggregates (Biggs et al., 2000; Li et al., 2021b).

For the weathered PBAT nanoplastics, the presence of 10 mg/L BSA did not affect the aggregation: weathered PBAT nanoplastics remained stable under all electrolyte concentrations (Fig. 3B). Further increase of BSA concentration did not lead to aggregation of weathered PBAT nanoplastics in either 1000 mM NaCl nor 50 mM CaCl<sub>2</sub> (Figure S5C,D).

However,  $\zeta$ -potentials of weathered PBAT nanoplastics became less negative in the presence of BSA, and the classical DLVO theory predicted attractive interactions between weathered PBAT nanoplastics in NaCl (> 100 mM) and CaCl<sub>2</sub> (> 2 mM). This discrepancy is consistent with the discrepancy observed for weathered PBAT nanoplastics in pure electrolyte solutions, suggesting the dominant role of surface roughness to stabilize weathered PBAT nanoplastics.

### 3.4. Aggregation of pristine and weathered PBAT nanoplastics in the presence of lysozyme (LSZ)

The presence of 10 mg/L LSZ promoted the aggregation of pristine PBAT nanoplastics under all electrolyte concentrations (Figure S6). It has been reported that LSZ could induce aggregation of silica particles through bridging, which is related to the high positive excess charge density and low dipole moment of LSZ (Bharti et al., 2011). Besides, the positive charge of LSZ can neutralize the surface charge of pristine PBAT nanoplastics and reduces electrical double layer forces (Figure S7). However, further increase in electrolyte concentrations led to a slightly decreased effect of LSZ on aggregation, as  $\alpha$  at higher electrolyte concentrations became less than 1 relative to the  $\alpha$  at the lowest electrolyte concentrations (Fig. 3C). This is contradictory to the prediction made by DLVO (Figure S7B), where the interaction became more attractive as the electrolyte concentration increases. This could be due to the conformational changes of proteins, which are known to reduce attractive interactions between protein-coated surfaces at high electrolyte concentrations (Xu and Logan, 2005). Further increase in LSZ concentration enhanced the aggregation of pristine PBAT nanoplastics in 20 mM CaCl2 but not in 300 mM NaCl (Figure S8A,B), which is likely due to the bridging effect between Ca<sup>2+</sup> and LSZ-coated surfaces. Compared to BSA, LSZ promoted the aggregation of pristine PBAT nanoplastics to a larger extent, which can be attributed to the tendency of LSZ to form dimers that support the binding of LSZ-coated PBAT nanoplastics (Claesson et al., 1995).

Unlike the pristine PBAT nanoplastics, the weathered PBAT nanoplastics remained stable under most electrolyte concentrations in the presence of 10 mg/L LSZ, and only slightly aggregated in < 10 mM CaCl $_{\rm 2}$  (Fig. 3D). This again demonstrated the high stability of weathered PBAT nanoplastics that was inherently controlled by the surface roughness of the nanoplastics and unlikely be affected by the presence of proteins. Nonetheless, the presence of LSZ at low concentrations of CaCl $_{\rm 2}$  slightly promoted the aggregation of weathered PBAT nanoplastics, likely caused by the bridging between Ca $^{\rm 2+}$  and LSZ-coated surfaces. In addition, further increase in LSZ did not trigger aggregation of weathered PBAT nanoplastic in 1000 mM NaCl nor in 50 mM CaCl $_{\rm 2}$  (Figure S8C,D).

### 3.5. Stability of PBAT nanoplastics in natural waters

Aggregation and stability of pristine and weathered PBAT nanoplastics were explored in soil pore water, freshwater, and seawater (Fig. 4). In the soil pore water, pristine PBAT nanoplastics showed weak aggregation, which is likely caused by the relatively high concentration of Ca<sup>2+</sup> (3.3 mM) in the soil pore water (Table S2). While this is lower than the experimentally determined CCC in CaCl<sub>2</sub> (i.e., 20 mM), other ions, i.e., Na<sup>+</sup>, K<sup>+</sup>, Mg<sup>2+</sup>, Cl<sup>-</sup>, and SO<sub>4</sub><sup>2-</sup> also contribute to the ionic strength, causing the weak aggregation. In the freshwater (river water), no aggregation of pristine PBAT nanoplastics was observed, consistent with the low electrolyte concentrations in the water. In the seawater, however, pristine PBAT nanoplastics showed pronounced aggregation, which is caused by the high concentrations of Na<sup>+</sup> (176.1 mM), K<sup>+</sup> (7.6 mM), Mg<sup>2+</sup> (21.6 mM), and Ca<sup>2+</sup> (6.3 mM), contributing to an ionic strength readily exceeding the CCC (Table S2). In contrast to the pristine PBAT nanoplastics, the weathered PBAT nanoplastics did not show aggregation in any of the water samples, consistent with its high stability observed in NaCl and CaCl2. Overall, the aggregation of pristine and weathered PBAT nanoplastics in natural waters followed the trend observed in the aggregation kinetic experiments.

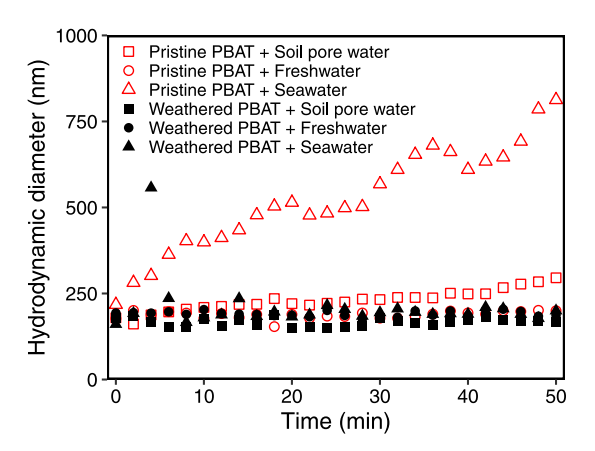


**Fig. 4.** Aggregation profiles of pristine (open symbols) and weathered (solid symbols) PBAT nanoplastics in natural waters. Data represent the average of two replicates.

### 4. Conclusions

Our study showed that, in general, pristine and weathered biodegradable (PBAT) nanoplastics form highly stable suspensions in aquatic environments. When exposed to environmental conditions, proteins can sorb onto the surfaces of nanoplastics, thereby modifying the surface properties and colloidal stability of the particles. While the presence of negative-charged proteins (i.e., BSA) only slightly promoted the aggregation of pristine PBAT nanoplastics, the presence of positive-charged proteins (i.e., LSZ) profoundly promoted the aggregation of pristine PBAT nanoplastics. This highlights the distinctively different role of negative-charged and positive-charged proteins and the importance of eco-coronas in controlling the colloidal stability of nanoplastics. However, neither the negative-charged proteins (i.e., BSA) nor the positivecharged (i.e., LSZ) proteins could promote aggregation of weathered PBAT nanoplastics under most experimental conditions, suggesting the more dominate role of weathering on determining the environmental fate of nanoplastics.

In natural waters, organic and inorganic compounds will interact with biodegradable nanoplastics, affecting their aggregation behavior and stability. In both soil pore water and river water, pristine and weathered PBAT nanoplastics are highly stable, suggesting that these nanoplastics can be transported through terrestrial and freshwater systems to the ocean. Once entering the marine environment, the increased ionic strength destabilizes the pristine PBAT nanoplastics, but not the weathered PBAT nanoplastics. Nonetheless, this study shows that biodegradable nanoplastics have a high colloidal stability and thus have the potential to be mobile in terrestrial and freshwater systems, which may facilitate their migration to the aquatic environment, where they may become persistent pollutants due to limited degradability. Therefore, it is important to appropriately dispose and manage biodegradable plastic wastes, preventing the exposure of biodegradable plastics to the aquatic environment.

### Supporting information

Supporting information includes details on DLVO calculations, experimental conditions for aggregation kinetics of pristine and weathered PBAT nanoplastics, chemical composition of natural water samples, aggregation profiles of pristine and weathered PBAT nanoplastics, and DLVO interaction energy profiles between PBAT nanoplastics.

### CRediT authorship contribution statement

**Yingxue Yu:** Conceptualization, Writing – original draft, Methodology, Data collection, Formal analysis, Visualization, Writing – review

Y. Yu et al. Water Research 239 (2023) 120018

& editing. Anton F. Astner: Methodology, Writing – review & editing. Tahsin Md. Zahid: Methodology, Writing – review & editing. Indranil Chowdhury: Methodology, Writing – review & editing. Douglas G. Hayes: Methodology, Writing – review & editing. Markus Flury: Conceptualization, Writing – original draft, Methodology, Formal analysis, Writing – review & editing.

### Declaration of competing interest

The authors declare that they have no known competing financial interests or personal relationships that could have appeared to influence the work reported in this paper.

#### Data availability

Data will be made available on request.

### Acknowledgments

This work was supported by National Science Foundation Grant 2152514 from the NSF-EAR Geobiology and Low-Temperature Geochemistry program. We thank Valerie Lynch-Holm from the WSU Franceschi Microscopy and Imaging Center for her help with the electron microscopy.

### Appendix A. Supplementary data

Supplementary material related to this article can be found online at https://doi.org/10.1016/j.watres.2023.120018.

#### References

- Astner, A.F., Hayes, D.G., O'Neill, H., Evans, B.R., Pingali, S.V., Urban, V.S., Young, T.M., 2019. Mechanical formation of micro- and nano-plastic materials for environmental studies in agricultural ecosystems. Sci. Total Environ. 685, 1097–1106.
- Badaire, S., Cottin-Bizonne, C., Stroock, A.D., 2008. Experimental investigation of selective colloidal interactions controlled by shape, surface roughness, and steric layers. Langmuir 24, 11451–11463.
- Berg, J.C., 2010. An Introduction to Interfaces and Colloids. The Bridge to Nanoscience. World Scientific, Hackensack, New Jersey.
- Bharti, B., Meissner, J., Findenegg, G.H., 2011. Aggregation of silica nanoparticles directed by adsorption of lysozyme. Langmuir 27, 9823–9833.
- Biggs, S., Habgood, M., Jameson, G.J., et al., 2000. Aggregate structures formed via a bridging flocculation mechanism. J. Chem. Eng. 80, 13–22.
- Chen, K.L., Mylon, S.E., Elimelech, M., 2006. Aggregation kinetics of alginate-coated hematite nanoparticles in monovalent and divalent electrolytes. Environ. Sci. Technol. 40, 1516–1523.
- Claesson, P.M., Blomberg, E., Fröberg, J.C., Nylander, T., Arnebrant, T., 1995. Protein interactions at solid surfaces. Adv. Colloid Interface Sci. 57, 161–227.
- Cole, M., Galloway, T.S., 2015. Ingestion of nanoplastics and microplastics by Pacific oyster larvae. Environ. Sci. Technol. 49, 14625–14632.
- Dong, Z., Hou, Y., Han, W., Liu, M., Wang, J., Qiu, Y., 2020. Protein corona-mediated transport of nanoplastics in seawater-saturated porous media. Water Res. 115978. http://dx.doi.org/10.1016/j.watres.2020.115978.
- Elimelech, M., Gregory, J., Jia, X., Williams, R.A., 1995. Particle Deposition and Aggregation: Measurement, Modelling, and Simulation. Butterworth-Heinemann, Oxford.
- Espinosa, C., Beltrán, J.M.G., Esteban, M.A., Cuesta, A., 2018. In vitro effects of virgin microplastics on fish head-kidney leucocyte activities. Environ. Pollut. 235, 30–38.
- Flury, M., Narayan, R., 2021. Biodegradable plastic as integral part of the solution to plastic waste pollution of the environment. Curr. Opin. Green Sustain. Chem. 30, 100490. http://dx.doi.org/10.1016/j.cogsc.2021.100490.
- Gewert, B., Plassmann, M., Sandblom, O., MacLeod, M., 2018. Identification of chain scission products released to water by plastic exposed to ultraviolet light. Environ. Sci. Technol. 5, 272–276.
- Geyer, R., Jambeck, J.R., Law, K.L., 2017. Production, use, and fate of all plastics ever made. Sci. Adv. 3, e1700782. http://dx.doi.org/10.1126/sciadv.1700782.

- González-Pleiter, M., Tamayo-Belda, M., Pulido-Reyes, G., Amariei, G., Leganés, F., Rosal, R., Fernández-Piñas, F., 2019. Secondary nanoplastics released from a biodegradable microplastic severely impact freshwater environments. Environ. Sci. Nano 6, 1382–1392.
- Haider, T.P., Volker, C., Kramm, J., Landfester, K., Wurm, F.R., 2019. Plastics of the future? The impact of biodegradable polymers on the environment and on society. Angew. Chem. Int. Ed. 58, 50–62.
- Hayes, D.G., Wadsworth, L.C., Sintim, H.Y., Flury, M., English, M., Schaeffer, S., Saxton, A.M., 2017. Effect of diverse weathering conditions on the physicochemical properties of biodegradable plastic mulches. Polym. Test 62, 454–467.
- Holthoff, H., Egelhaaf, S.U., Borkovec, M., Schurtenberger, P., Sticher, H., 1996.Coagulation rate measurements of colloidal particles by simultaneous static and dynamic light scattering. Langmuir 12, 5541–5549.
- Huangfu, X., Jiang, J., Ma, J., Liu, Y., Yang, J., 2013. Aggregation kinetics of manganese dioxide colloids in aqueous solution: Influence of humic substances and biomacromolecules. Environ. Sci. Technol. 47, 10285–10292.
- Kubowicz, S., Booth, A.M., 2017. Biodegradability of plastics: Challenges and misconceptions. Environ. Sci. Technol. 51, 12058–12060.
- Lan, Y., Caciagli, A., Guidetti, G., Yu, Z., Liu, J., Johansen, V.E., Kamp, M., Abell, C., Vignolini, S., Scherman, O.A., et al., 2018. Unexpected stability of aqueous dispersions of raspberry-like colloids. Nat. Commun. 9, 1–8. http://dx.doi.org/10. 1038/s41467--018--05560--3.
- Law, K.L., 2017. Plastics in the marine environment. Ann. Rev. Mar. Sci. 9, 205-229.
- Li, X., He, E., Jiang, K., Peijnenburg, W.J., Qiu, H., 2021a. The crucial role of a protein corona in determining the aggregation kinetics and colloidal stability of polystyrene nanoplastics. Water Res. 190, 116742. http://dx.doi.org/10.1016/j. watres.2020.116742.
- Li, X., He, E., Xia, B., Liu, Y., Zhang, P., Cao, X., Zhao, L., Xu, X., Qiu, H., 2021b. Protein corona-induced aggregation of differently sized nanoplastics: Impacts of protein type and concentration. Environ. Sci. Nano 8, 1560–1570.
- Liu, Y., Hu, Y., Yang, C., Chen, C., Huang, W., Dang, Z., 2019. Aggregation kinetics of UV irradiated nanoplastics in aquatic environments. Water Res. 163, 114870. http://dx.doi.org/10.1016/j.watres.2019.114870.
- Mistretta, M.C., La Mantia, F.P., Titone, V., Megna, B., Botta, L., Morreale, M., 2019.
  Durability of biodegradable polymers for the conservation of cultural heritage.
  Front. Mater. Sci. 6, 151. http://dx.doi.org/10.3389/fmats.2019.00151.
- Narancic, T., Verstichel, S., Chaganti, S.Reddy., Morales-Gamez, L., Kenny, S.T., Wilde, B.De., Padamati, R.Babu., O'Connor, K.E., 2018. Biodegradable plastic blends create new possibilities for end-of-life management of plastics but they are not a panacea for plastic pollution. Environ. Sci. Technol. 52, 10441–10452.
- Nithin, B., Goel, S., 2017. Degradation of plastics. In: Advances in Solid and Hazardous Waste Management. Springer, pp. 235–247.
- Prata, J.C., 2018. Airborne microplastics: Consequences to human health? Environ. Pollut. 234, 115–126.
- Qin, Q., Yang, Y., Yang, C., Zhang, L., Yin, H., Yu, F., Ma, J., 2022. Degradation and adsorption behavior of biodegradable plastic PLA under conventional weathering conditions. Sci. Total Environ. 842, 156775. http://dx.doi.org/10.1016/j.scitotenv. 2022.156775.
- Ryan, P.G., 2018. Entanglement of birds in plastics and other synthetic materials. Mar. Pollut. Bull. 135, 159–164.
- Saleh, N.B., Pfefferle, L.D., Elimelech, M., 2010. Influence of biomacromolecules and humic acid on the aggregation kinetics of single-walled carbon nanotubes. Environ. Sci. Technol. 44, 2412–2418.
- Shams, M., Alam, I., Chowdhury, I., 2020. Aggregation and stability of nanoscale plastics in aquatic environment. Water Res. 171, 115401. http://dx.doi.org/10. 1016/j.watres.2019.115401.
- Sheng, A., Liu, F., Xie, N., Liu, J., 2016. Impact of proteins on aggregation kinetics and adsorption ability of hematite nanoparticles in aqueous dispersions. Environ. Sci. Technol. 50, 2228–2235.
- Sintim, H.Y., Bary, A.I., Hayes, D.G., English, M.E., Schaeffer, S.M., Miles, C.A., Zelenyuk, A., Suski, K., Flury, M., 2019. Release of micro- and nanoparticles from biodegradable plastic during in situ composting. Sci. Total Environ. 675, 686–693.
- Sintim, H.Y., Bary, A.I., Hayes, D.G., Wadsworth, L.C., Anunciado, M.B., English, M.E., Bandopadhyay, S., Schaeffer, S.M., DeBruyn, J.M., Miles, C.A., Reganold, J.P., Flury, M., 2020. In situ degradation of biodegradable plastic mulch films in compost and agricultural soils. Sci. Total Environ. 727, 138668. http://dx.doi.org/10.1016/ j.scitotenv.2020.138668.
- Tosin, M., Pischedda, A., Degli-Innocenti, F., 2019. Biodegradation kinetics in soil of a multi-constituent biodegradable plastic. Polym. Degrad. Stab. 166, 213–218.
- Wang, X., Li, Y., Zhao, J., Xia, X., Shi, X., Duan, J., Zhang, W., 2020. UV-induced aggregation of polystyrene nanoplastics: Effects of radicals, Surface Functional Groups and Electrolyte. Environ. Sci. Nano 7, 3914–3926.

- Wang, X.W., Wang, G.X., Huang, D., Lu, B., Zhen, Z.C., Ding, Y., Ren, Z.L., Wang, P.L., Zhang, W., Ji, J.H., 2019. Degradability comparison of poly(butylene adipate terephthalate) and its composites filled with starch and calcium carbonate in different aquatic environments. J. Appl. Polym. Sci. 136, 46916. http://dx.doi.org/10.1002/APP.46916.
- Wei, X., Bohlén, M., Lindblad, C., Hedenqvist, M., Hakonen, A., 2021. Microplastics generated from a biodegradable plastic in freshwater and seawater. Water Res. 198, 117123. http://dx.doi.org/10.1016/j.watres.2021.117123.
- Xu, L., Logan, B.E., 2005. Interaction forces between colloids and protein-coated surfaces measured using an atomic force microscope. Environ. Sci. Technol. 39, 3592–3600.
- Yang, W., Shang, J., Sharma, P., Li, B., Liu, K., Flury, M., 2019. Colloidal stability and aggregation kinetics of biochar colloids: Effects of pyrolysis temperature, cation type, and humic acid concentrations. Sci. Total Environ. 658, 1306–1315.
- Yu, Y., Griffin-LaHue, D.E., Miles, C.A., Hayes, D.G., Flury, M., 2021. Are microplastics from biodegradable plastic mulches an environmental concern? J. Hazard. Mater. Adv. 4, 100024. http://dx.doi.org/10.1016/j.hazadv.2021.100024.